Mon. Not. R. Astron. Soc. **345,** 1133–1144 (2003)

Searching for the physical drivers of eigenvector 1: influence of black hole mass and Eddington ratio

Paola Marziani,[1⋆] Radoslav K. Zamanov,[1⋆†] Jack W. Sulentic[2⋆] and Massimo Calvani[1⋆]

[1]*Istituto Nazionale di Astrofisica, Osservatorio Astronomico di Padova, Vicolo dell'Osservatorio 5, I-35122 Padova, Italy*
[2]*Department of Physics and Astronomy, University of Alabama, Tuscaloosa, AL 35487, USA*

Accepted 2003 July 17. Received 2003 July 16; in original form 2003 May 20

ABSTRACT

We compute the virial mass (M) of the central black hole and the luminosity-to-mass (L/M) ratio of ≈300 low-z quasars and luminous type 1 Seyfert nuclei. We analyse the following: (1) whether radio-quiet and radio-loud objects show systematic differences in terms of M and L/M; (2) the influence of M and L/M on the shape of the Hβ broad component line profile; and (3) the significance of the so-called 'blue outliers', i.e. sources showing a significant blueshift of the [O III] λλ4959,5007 lines with respect to the narrow component of Hβ, which is used as an estimator of the quasar reference frame. We show that M and L/M distributions for radio-quiet and radio-loud sources are probably different for samples matched in luminosity and redshift, in the sense that radio-quiet sources have systematically smaller masses and larger L/M. However, the L/M ratio distributions become indistinguishable if $8.5 < \log M < 9.5$. Line profile comparisons for median spectra computed over narrow ranges of M and L/M indicate that a Lorentz function provides a better fit for higher L/M sources and a double Gaussian for lower L/M values. A second (redshifted) Gaussian component at low L/M appears as a red asymmetry frequently observed in radio-loud and radio-quiet sources with broader (full width at half-maximum $\gtrsim$4000 km s^{-1}) Hβ broad component profiles. This component becomes stronger in larger mass and lower L/M sources. No specific influence of radio loudness on the Hβ broad component profile is detected, although equivalent widths of Hβ broad component and especially of [O III] λλ4959,5007 are larger for radio-loud sources. We identify five more 'blue outlier' sources. Since these sources are, on average, one magnitude brighter than other active galactic nuclei with similar mass, their resulting Eddington ratio is 2–3 times higher. We hint at evolutionary effects that explain some of these results, and reinforce the 'eigenvector 1' correlations.

Key words: galaxies: active – quasars: emission lines – quasars: general.

1 INTRODUCTION

Studies of emission lines play an important role in our understanding of active galactic nuclei (AGN) and the physics of accretion processes, although the connection between the main theoretical parameters (i.e. black hole mass, accretion rates, black hole spin and viewing angle) and observed spectral parameters is, at best, just sketchy and qualitative. In recent years, a major innovation has been ascribed to the so-called 'eigenvector 1' (E1) correlations (Boroson & Green 1992). The original E1 was most closely related to the anticorrelation between Fe II$_{opt}$ strength and peak [O III] λ5007 intensity, and the full width at half-maximum (FWHM) of the Hβ broad component (Hβ_{BC}).

E1-related correlations have emerged as very robust, since they continue to appear in different low-z AGN samples, even if a set of spectral parameters partly different from the ones used for the original principal component analysis (PCA) by Boroson & Green (1992) is considered. An outstanding relationship in the context of E1 involves the FWHM(Hβ_{BC}) and the ratio between the equivalent width W of the Fe II$_{opt}$ complex centred at λ4570 and Hβ_{BC}, $R_{Fe\,II} = W(\text{Fe II } \lambda4570)/W(\text{H}\beta_{BC})$. Low-redshift AGN occupy an elbow sequence in the plane defined by these two parameters (see Sulentic, Marziani & Dultzin-Hacyan 2000a; Marziani et al. 2001).

⋆E-mail: marziani@pd.astro.it (PM); zamanov@pd.astro.it, rz@astro.livjm.ac.uk (RKZ); giacomo@merlot.astr.ua.edu (JWS); calvani@pd.astro.it (MC)
†Present address: Astrophysics Research Institute, Liverpool John Moores University, Twelve Quays House, Egerton Wharf, Birkenhead CH41 1LD.

The overall sequence is defined by radio-quiet (RQ) sources, while the radio¨-loud (RL) AGN occupy only a restricted part of it. The domain where FWHM(H$\beta_{\rm BC}$) $\lesssim$ 4000 km s^{-1} is predominantly occupied by RQ sources (Sulentic et al. 2000a; see also Sulentic et al. 2003). There is an apparent dichotomy in the H$\beta_{\rm BC}$ line profile shapes: sources with FWHM(H$\beta_{\rm BC}$) $\lesssim$ 4000 km s^{-1} show typically a Lorentzian H$\beta_{\rm BC}$, while for FWHM(H$\beta_{\rm BC}$) $\gtrsim$ 4000 km s^{-1} a double Gaussian fit is more appropriate (Sulentic et al. 2002); the so-called 'blue outliers' (sources showing a significant blueshift of the [O III] $\lambda\lambda$4959,5007 lines with respect to inferred quasar frame) occur among sources with strongest Fe II λ4570 and narrowest H$\beta_{\rm BC}$ (Zamanov et al. 2002; Marziani et al. 2003a).

The robustness of the E1 correlations probably stems from a series of concurring factors: (1) an Eddington ratio that may be continuously changing along the E1 sequence (e.g. Boroson, Persson & Oke 1985; Boroson & Green 1992; Murray et al. 1995; Nicastro 2000; Marziani et al. 2001; Boroson 2002); (2) outflow/wind properties that are expected to depend on Eddington ratio (e.g. Dultzin-Hacyan, Marziani & Sulentic 2000; Marziani et al. 2001); (3) orientation effects that will blur any physical correlation and displace sources in the direction of increasing Eddington ratio (Marziani et al. 2001; see also, Nagao, Taniguchi & Murayama 2000; Zhou et al. 2003); (4) broad-line region (BLR) structural effects (Sulentic et al. 2000b, 2002; see also Gaskell et al. 1999); and (5) last, but not least, evolutionary effects that will lead to an increase of black hole mass as well as of the [O III] λ5007 rest-frame equivalent width (Zamanov et al. 2002; Boroson 2002). We will briefly discuss them in Sections 8.4 and 9.

Even if there is not yet a consensus (see e.g. Marziani et al. 2001; Boroson 2002), the physical drivers of E1 are likely to involve the luminosity-to-black hole mass ratio ($L/M \propto$ Eddington ratio), an orientation angle, and the black hole mass (M) (Zamanov & Marziani 2002). Additional properties such as black hole spin (e.g. Wilson & Colbert 1995) or the properties of the host galaxy environment (e.g. McLure et al. 1999) are also likely to play a role in any RQ–RL dichotomy.

This paper presents a basic investigation of the influence of L/M and M on RL and RQ sample properties, on the H$\beta_{\rm BC}$ line profile, and on the occurrence of the 'blue outliers', which are all major E1-dependent phenomena. The paper is organized as follows. In Section 2 we present our quasar sample, followed by a derivation of M and L/M in Section 3. In Section 4 we present and discuss mass–luminosity diagrams. Section 5 contains a comparison of radio-quiet and radio-loud sources. An analysis of H$\beta_{\rm BC}$ profiles follows in Section 6, as well as the significance of the 'blue outlier' sources in Section 7. Our results are discussed in Section 8. Section 9 provides some concluding remarks.

2 SAMPLE DEFINITION AND MEASUREMENTS

We use the spectra of 278 AGNs. Our AGN sample includes 215 sources and has been presented elsewhere (Marziani et al. 2003b, hereafter M03). We added 63 soft X-ray selected sources with suitable optical spectroscopic data (Grupe et al. 1999, hereafter G99) because this turns out to be the most fertile source of 'blue outliers'. Inclusion of Grupe et al.'s data makes our sample less biased, as described in Section 5.4. The optical characteristics of these X-ray selected sources include: (1) relatively 'narrow' broad emission lines, e.g. narrow-line type 1 Seyfert (NLSy1) sources; (2) strong optical Fe II$_{\rm opt}$ blends; and (3) weak forbidden emission lines. The merged data sets provide reasonable-quality spectra (signal-to-noise ratio S/N $\approx$ 20–70) for the region near Hβ in 278 AGN ($z \lesssim 0.8$). The M03 data set is not complete (see M03 for discussion of completeness and sample biases).

We use line parameters reported in M03 and derive the corresponding measures (using the same procedures described in M03) for the X-ray selected sample from the digital spectra made publicly available by G99. We consider here measurements of the following parameters: (a) FWHM(H$\beta_{\rm BC}$); (b) equivalent width ratio $R_{\rm Fe\,II} = W$(Fe II λ4570)$/W$(H$\beta_{\rm BC}$); (c) FWHM measurement of the lines in the Fe II λ4570 blend (see M03 for details); and (d) radial velocity difference between [O III] λ5007 and Hβ at the line peak (without narrow component subtraction). The accuracy of the G99 wavelength calibration was evaluated by examining the distribution of radial velocity difference between[[O III] λ4959 and [O III] λ5007. Whenever possible, [O III] λ4363 was also used and all inter-narrow-line differences were found to be comparable to our measures (cf. Zamanov et al. 2002).

Apparent (m_V) and absolute B magnitudes (M_B) were taken from the tenth edition of the AGN catalogue (Véron-Cetty & Véron 2001). A magnitude correction + 0.88 mag was applied to convert M_B from $H_0 = 50$ km s^{-1} Mpc^{-1} to $H_0 = 75$ km s^{-1} Mpc^{-1} ($q_0 = 0$), which we use throughout this paper. Galactic extinction values A_B were taken from NED following Schlegel, Finkbeiner & Davis (1998). Sources were considered RL if the specific flux at 6 cm and in the B band was larger than 10, with data taken from the Véron-Cetty & Véron (2001) catalogue.

3 COMPUTATION OF M AND L/M

3.1 Black hole masses

One can estimate the mass of the putative supermassive black hole using FWHM(H$\beta_{\rm BC}$) and a reverberation 'radius' (Kaspi et al. 2000) along with the assumption of virialized motions. It is now common to estimate the mass by assuming the BLR distance from the central continuum source $r_{\rm BLR} \propto (L_{5100})^{\alpha}$ and $\alpha = 0.7$, as derived from the reverberation data (Kaspi et al. 2000). The virial mass is $M = r_{\rm BLR} v^2/G$, where $v = (\sqrt{3}/2)$FWHM(H$\beta_{\rm BC}$) (cf. Woo & Urry 2002a), and G is the gravitational constant. We can therefore write the black hole virial mass as

$$M = 4.817 \times \left[\frac{\rm FWHM(H\beta_{BC})}{1\ {\rm km\ s^{-1}}}\right]^2 \left(\frac{\lambda L_{5100}}{10^{44}\ {\rm erg\ s^{-1}}}\right)^{0.7}, \quad (1)$$

where M is in solar units, L_{5100} is the specific luminosity at 5100 Å (in units of erg s^{-1} cm^{-2} Å^{-1}), and

$$\lambda L_{5100} = 3.137 \times 10^{35-0.4(M_B - A_B)}\ {\rm erg\ s^{-1}}. \quad (2)$$

In order to convert the absolute B magnitude M_B to λL_{5100}, we assumed that the specific flux is $f_\nu \propto \nu^{-0.3}$. The derived masses are thought to be reasonable estimates within a factor of about 2–3 (see also Woo & Urry 2002a; Vestergaard 2002).

3.2 Influence of orientation

Source viewing angle is especially important in AGN where the concepts of disc accretion/line emission and jet ejection are widely favoured. In the above mass derivation formula we did not include any orientation-related broadening factor. If H$\beta_{\rm BC}$ is emitted in a highly flattened structure, then M can be underestimated by a factor $\approx \sin i^{-2}$ in pole-on/face-on sources (i.e. with accretion disc axis oriented along our line of sight). Unfortunately, we do not yet have a proper way to estimate the viewing angle i for each source. This is a

major drawback because there is observational evidence suggesting that orientation can affect linewidth by a factor ≈2 (Brotherton 1996; Marziani et al. 2001; Jarvis & McLure 2002). Even though we neglected the effects of orientation in the general sample population, we considered it in computations of M and L/M for the relatively rare and extreme class that is likely observed close to 'pole-on': the 'blue outliers' (Section 7.3).

3.3 The role of the BLR size–luminosity relationship

The exponent in the relationship between source luminosity L and $r_{\rm BLR}$ is assumed to be $\alpha = 0.7$. Any deviation from this value has quantitative effects on our results. Our sample includes many moderately luminous quasars at $0.4 < z < 0.8$, so it is important to stress that the relationship derived by Kaspi et al. (2000) is based exclusively on quasars of $z < 0.4$ and that the high- (and low-) luminosity ranges of the correlation are poorly sampled.

If we consider sources in the luminosity range $43.4 \lesssim \log(L/{\rm L}_\odot) \lesssim 45$ (i.e. where we have uniform luminosity sampling), the slope of the best fit is $\alpha = 0.8$, and could easily be as high as $\alpha = 1$ without increasing significantly the fit standard deviation. Marziani et al. (2001) considered this case, which seems appropriate for the Palomar-Green (PG) quasar luminosity range. One must remain open to the possibility that $0.5 \lesssim \alpha \lesssim 1$, and that α might even be a function of L. Changing α implies an L-dependent change in mass estimates; therefore the slope of the luminosity-to-mass relationship (Fig. 1) is affected as well as the location of points in the L/M versus M diagram (Figs 7 and 12). Despite these possibilities, the systematic trends discussed in this paper should not be affected.

3.4 Bolometric luminosity

We calculated the bolometric luminosity L from $L \approx 10\lambda L_\lambda(5100\text{Å})$ (details can be found in Elvis et al. 1994; Wandel, Peterson & Malkan 1999; Collin et al. 2002). Values computed in this way were used to derive the L/M ratio. The L/M ratio everywhere is expressed in solar units with the solar value $(L/M)_\odot = 1.92$ erg s^{-1} g^{-1}, and the Eddington limit corresponding to $\log L/M = 4.53$.

We neglected any possible differences in the spectral energy distribution (SED) between source subclasses. In order to test this benign neglect, we considered 44 sources that are common with Woo & Urry (2002a) where SEDs were constructed from archival data. Comparison of our bolometric luminosity values showed no significant systematic difference: $\Delta\overline{\log L} \approx -0.06$ for all 44 sources, with a standard deviation $\sigma \approx 0.24$. RQ sources show $\Delta\overline{\log L} \approx -0.06$ with $\sigma \approx 0.22$, while RL show $\Delta\overline{\log L} \approx -0.07$ with a slightly larger $\sigma \approx 0.26$. If we consider separately RQ and RL sources with the restriction FWHM(H$\beta_{\rm BC}$) $\geqslant$ 4000 km s^{-1} (see Section 5.3), we find $\Delta\overline{\log L} \approx -0.05$ (RQ) and $\Delta\overline{\log L} \approx -0.01$ (RL). It is worth noting that the scatter is due to a minority of badly behaving data points (≈20 per cent). If they are removed, the standard deviation becomes $\sigma \approx 0.1$ in all cases, with systematic differences always $\lesssim 0.05$.

4 MASS–LUMINOSITY DIAGRAM

Fig. 1 shows a plot of M_B versus M for our combined sample, which covers an absolute B magnitude range $-20 \lesssim M_B \lesssim -27$ and an estimated black hole mass range $10^7 \lesssim M \lesssim 10^{10}$ (M is everywhere given in M$_\odot$). The data show a rather well-defined range in L/M with almost all sources lying between $0.02 \lesssim L/L_{\rm Edd} \lesssim 1.00$. RQ sources show evidence for significant Malmquist bias, while RL sources show the opposite trend, probably related to a bias towards selecting higher-luminosity core-dominated sources likely to be beamed.

5 RADIO-LOUD AND RADIO-QUIET AGN

Table 1 presents average and median values of relevant properties for the RL and RQ subsamples. Kolmogorov–Smirnov tests indicate that RL and RQ samples differ significantly in redshift, m_V and absolute B magnitude distribution. The distributions of the computed parameters M and L/M are also significantly different for RQ and RL samples.

RL sources are somewhat over-represented in the M03 sample, but not in the M03 + G99 sample. Any over-representation can be properly quantified if we compare general population expectation for the number ratio between the number of RL sources and the total number of sources, i.e. $f_{\rm R} = {\rm N(RL)}/[{\rm N(RL)} + {\rm N(RQ)}]$, in the M_B range covered by our sample. Weighting the luminosity-dependent $f_{\rm R}$ value from La Franca et al. (1994) over the M_B distribution of our sample (see fig. 2 of M03), i.e. within $-27 < M_B < -23$, we obtain $f_{\rm R} \approx 25$ per cent versus $f_R \approx 39$ per cent in M03 and $f_{\rm R} \approx 26$ per cent in M03 + G99.

More cumbersome are the biases shown in Fig. 2: RL sources tend to be fainter and more distant than RQ ones, as well as intrinsically more luminous. The biases that are affecting RL sources are not clear. RL core-dominated sources are over-represented in M03. This will contribute to bias the RL sample to higher L and z values (for a more thorough discussion, see Sulentic et al. 2003).

5.1 Bootstrap simulations

Are differences in redshift and luminosity distributions the cause of the inferred M and L/M differences between RQ and RL sources?

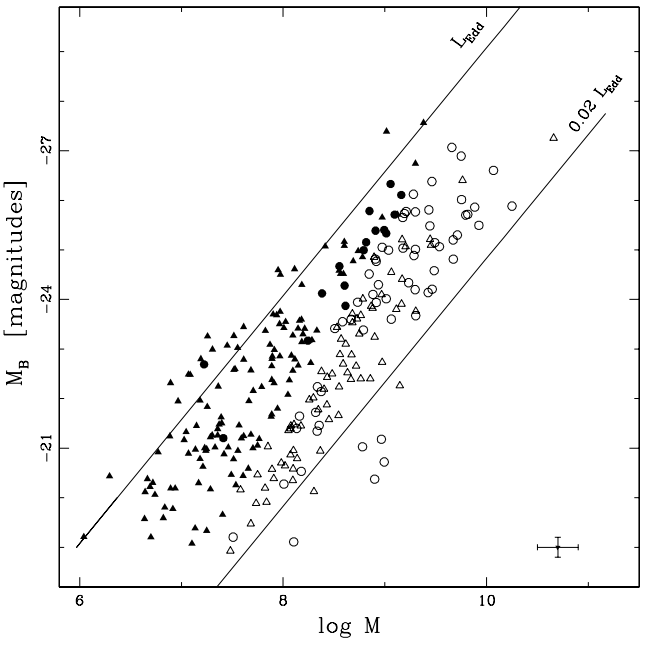

Figure 1. Distribution of absolute B magnitude (M_B) versus black hole mass M (in solar units) for the 278 AGN sample. M_B values are corrected for Galactic extinction. Triangles and circles indicate radio-quiet and radio-loud sources, respectively. Open symbols indicate sources with FWHM(H$\beta_{\rm BC}$) $\gtrsim$ 4000 km s^{-1}; filled symbols sources with FWHM(H$\beta_{\rm BC}$) $\lesssim$ 4000 km s^{-1} (see Section 5.4). The bars in the lower right corner indicate typical errors.

Table 1. RQ/RL sample averages and medians for redshift, apparent V magnitude (m_V), absolute B magnitude (M_B), BH mass (M), and luminosity-to-mass ratio. Average values are given with sample standard deviations, median values with first and third quartile values. $P_{\rm KS}$ is the probability that the two distributions are randomly drawn from the same parent population using Kolmogorov–Smirnov tests.

	N	z			m_V			M_B		
		Ave. $\pm\sigma$	Med. $^{75\,\rm per\,cent}_{25\,\rm per\,cent}$	$P_{\rm KS}$	Ave. $\pm\sigma$	Med. $^{75\,\rm per\,cent}_{25\,\rm per\,cent}$	$P_{\rm KS}$	Ave. $\pm\sigma$	Med. $^{75\,\rm per\,cent}_{25\,\rm per\,cent}$	$P_{\rm KS}$
RQ	202	0.13 ± 0.12	$0.089^{0.167}_{0.045}$	10^{-16}	15.5 ± 1.1	$15.5^{16.2}_{14.7}$	1.5×10^{-4}	-23.0 ± 1.8	$-23.0^{-21.6}_{-24.1}$	10^{-14}
RL	76	0.35 ± 0.21	$0.334^{0.530}_{0.200}$		16.1 ± 0.9	$16.1^{16.5}_{15.6}$		-24.8 ± 1.8	$-25.3^{-24.2}_{-26.2}$	

	M			L/M		
	Ave. $\pm\sigma$	Med. $^{75\,\rm per\,cent}_{25\,\rm per\,cent}$	$P_{\rm KS}$	Ave. $\pm\sigma$	Med. $^{75\,\rm per\,cent}_{25\,\rm per\,cent}$	$P_{\rm KS}$
RQ	8.21 ± 0.76	$8.21^{8.79}_{7.65}$	10^{-16}	3.89 ± 0.53	$3.95^{4.24}_{3.49}$	0.0017
RL	9.23 ± 0.60	$9.24^{9.67}_{8.92}$		3.65 ± 0.47	$3.63^{4.03}_{3.37}$	

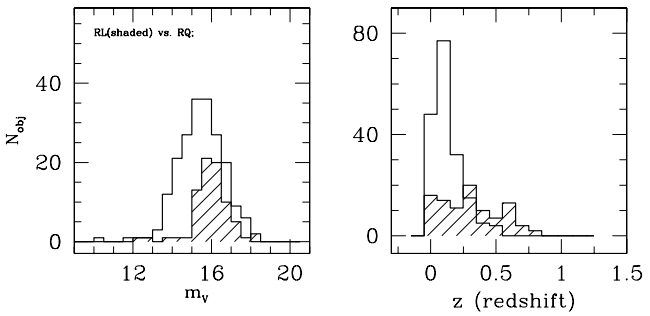

Figure 2. Distribution of apparent V magnitude (left panel) and redshift z (right panel) for our 278 AGN sample; shaded, RL; unshaded, RQ. The left panel shows that, in our sample, RL sources are on average less bright than RQ sources, while the right panel suggests a distribution favouring higher z for RL AGN.

We can use most of our sources in creating better-matched subsamples out of our M03 + G99 sample (bootstrap techniques, i.e. Efron & Tibshirani 1993). The most important parameter appears to be redshift (which implies a strong bound on the apparent magnitude). We constructed pseudo-samples of RQ and RL sources *with similar redshift and apparent magnitude distributions*. More precisely: (1) we randomly selected two pseudo-samples with the same z and m_V distributions, indistinguishable within a 2σ confidence limit; (2) we computed average $\log M$ and $\log L/M$ values for each pseudo-sample; (3) we repeated the selection $\sim$1000 times; (4) we computed the distribution of average $\log M$ and $\log L/M$ values for the pseudo-samples (the *bootstrapped* samples); (5) we derived the expectation values for $\langle\overline{\log M}\rangle$ and $\langle\overline{\log L/M}\rangle$ as the medians of the distributions for the bootstrapped samples; and (6) we estimated the significance level of any difference from the average values and the dispersion of the distributions. While we cannot eliminate biases from our sample, we can try to apply the same bias to both populations.

5.2 Matching z and m_V distributions

The bootstrap procedure makes both the M and L/M differences stronger (see the upper panels of Figs 3 and 4): the median values are $\langle\overline{\log M}(\rm RQ)\rangle \approx 8.07 \pm 0.07$ versus $\langle\overline{\log M}(\rm RL)\rangle \approx 8.81 \pm 0.06$, and $\langle\overline{\log L/M}(\rm RQ)\rangle \approx 3.88 \pm 0.05$ versus $\langle\overline{\log L/M}(\rm RL)\rangle \approx 3.45 \pm 0.06$. The results can be seen in Fig. 3 (the original sample) and Fig. 4 (after bootstrap simulations). Since matching m_V and z is equivalent to a match in L, it follows that the two plots are not independent,

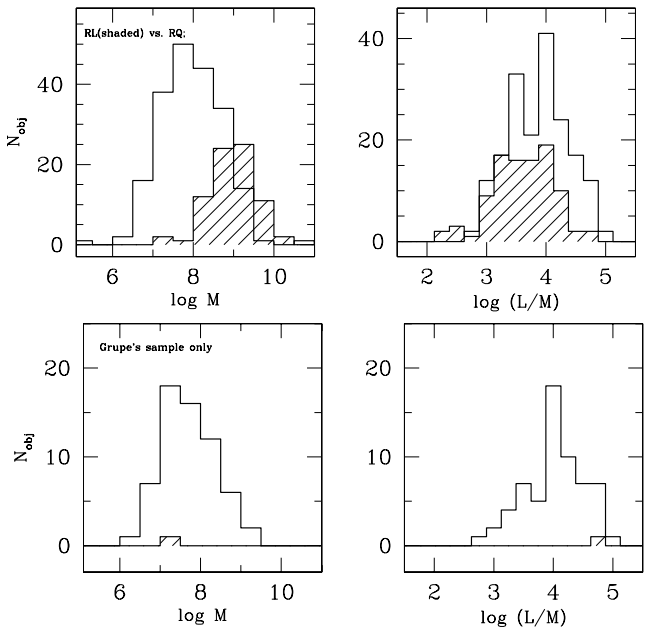

Figure 3. Distributions of M (left panels) and L/M ratio (right panels) for our sample (upper panels) and for the sample by Grupe et al. (1999) only (lower panels); shaded, RL; unshaded, RQ. The left panels show that RL sources show larger M than RQ, while the right panels suggest a largely overlapping L/M range for RQ and RL AGN, even if the largest L/M sources are almost all RQ.

and that systematically larger FWHM($\rm H\beta_{BC}$) drives a larger mass estimate for RL sources.

5.3 Same z and m_V distribution with a narrow mass range

To avoid sample biases, and to assess the reality of any L/M systematic difference, we restricted our attention to sources within a narrow mass range. At the same time, we retained the above conditions on the z and m_V distributions. The mass range was chosen so that we had the maximum possible number of sources: $8.5 \lesssim \log M \lesssim 9.5$ with 48 sources (Fig. 5). No systematic difference in $\log L/M$ ($\lesssim 0.2$) is found. In a comparison of RQ and RL sources with the additional condition FWHM($\rm H\beta_{BC}$) $\gtrsim 4000$ km s^{-1}, and matching the z and m_V distributions, we find again no systematic difference in either M or L/M distributions (see Fig. 6; note that the difference can be statistically significant, but it is of the order of the uncertainty in the M and L/M determination and therefore too small to be of relevance). The similarity of the parameter space occupation for RQ

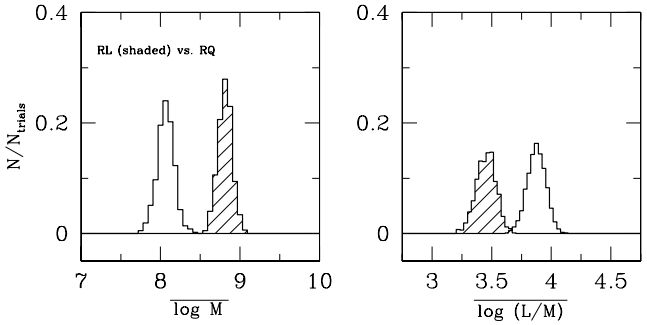

Figure 4. Results of bootstrap simulations. Distributions of average M (left) and L/M (right) for 1000 pseudo-samples of 40 RL (shaded) and RQ objects with matching apparent magnitude and redshift distribution. Bootstrap simulations suggest that there are systematic differences in the sense that RL sources have large M and lower L/M ratios than RQ AGN.

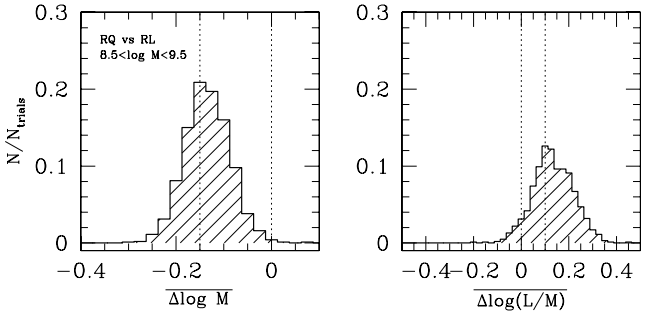

Figure 5. Distribution of $\Delta\overline{\log M} = \overline{\log M}(\mathrm{RQ}) - \overline{\log M}(\mathrm{RL})$ (left panel) and $\Delta\overline{\log L/M} = \overline{\log L/M}(\mathrm{RQ}) - \overline{\log L/M}(\mathrm{RL})$ (right panel) for ∼1000 pseudo-samples of RL and RQ sources. m_V and z distributions were matched, and a restriction to the M was applied: $8.5 \leqslant \log M \leqslant 9.5$ (48 sources). RL and RQ quasars have almost the same L/M ratio distributions.

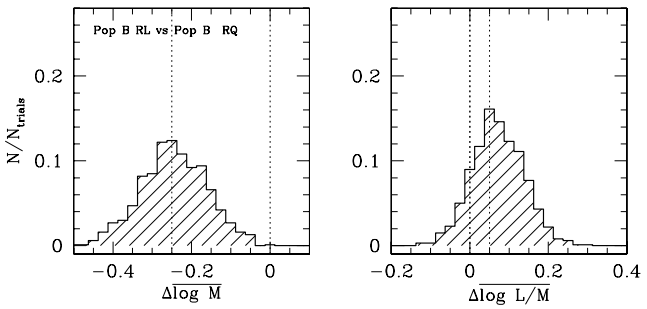

Figure 6. Distribution of $\Delta\overline{\log M}$ (left panels) and $\Delta\overline{\log L/M}$ (right panels) for ∼1000 pseudo-samples of 40 objects with FWHM($H\beta_{BC}$) $\geqslant$ 4000 km s^{-1} but separated on the basis of radio loudness. It points that RL and RQ Population B are not distinguishable on the basis of M or L/M.

and RL sources with FWHM($H\beta_{BC}$) $\gtrsim$ 4000 km s^{-1} carries into a similarity in derived L/M and M. In other words, there is a large RQ population whose M and L/M values are similar to the ones of RL sources.

5.4 Populations A and B: understanding biases

Sulentic et al. (2000a) introduced the concept of Population A [FWHM($H\beta_{BC}$) $\lesssim$ 4000 km s^{-1}] and Population B [FWHM($H\beta_{BC}$) $\gtrsim$ 4000 km s^{-1}] as fundamentally related to the BLR structural properties (Sulentic et al. 2000a,b). RQ sources dominate Population A (88 per cent of the total) and are about half of Population B sources. Most RL sources (≈75 per cent) are Population B. Thus to a large extent an RL versus RQ comparison is a Population A RQ versus Population B RL comparison [as it was in the early study on C IV λ1549 by Marziani et al. (1996)].

The validity of the previous results on M and L/M difference depends on (1) the fraction of Population A RQ sources at low z, and (2) whether most RL sources at $z < 1$ are Population B. A proper assessment of the Population A/Population B ratio for RQ samples would imply a thorough analysis of the discovery biases affecting major surveys (see e.g. Oshlack, Webster & Whiting 2002). This goes far beyond the aim of the present paper.

Actually, we know that we have a bias favouring Population A RQ sources in the G99 sample. If we apply the same bootstrap analysis to the M03 sample only, we obtain a lower fraction of Population A sources (≈45 per cent), but we reach the same qualitative conclusions. Therefore a significant bias may arise only if we *miss* a large fraction of Population B RQ sources (>20 per cent). This does not seem the case. An analysis of the SDSS shows that NLSy1s should be ≈15 per cent of all low-z AGN (Williams, Pogge & Mathur 2002). The ratio between NLSy1s and the rest of Population A, i.e. sources satisfying the criterion 2000 km s^{-1} $\lesssim$ FHWM($H\beta_{BC}$) $\lesssim$ 4000 km s^{-1}, is ≈ one-third (estimated on the whole M03 sample, on a restriction to PG sources). This implies that Population A should be ≈60 per cent of all low-z AGN. We note that: (a) in M03 + G99, Population A sources account for ≈52 per cent of all sources; (b) the ratio of NLSy1s to all RQ sources is ≈15–20 per cent if we consider the M03 and M03 + G99 independently, in line with the SDSS findings. Therefore, if there is a sample bias favouring one of the two populations, it is not strong.

Regarding the second issue, it has been possible to show that Fanaroff–Riley type II (FRII) quasars belong exclusively to Population B. RL sources with narrower lines [RL with FWHM($H\beta_{BC}$) $\lesssim$ 4000 km s^{-1}] are predominantly core-dominated (CD) sources, and therefore likely to be a less frequent, beamed population of preferentially aligned sources in an FRII/CD unification scenario (Sulentic et al. 2003).

Even if the amplitude of the L/M and M systematic difference depends on sample definition, such a difference is unlikely to be caused by selection effects, and should be considered real. This is in line with recent research pointing towards systematic differences in the mass function of RQ and RL AGN (as discussed in Section 8.2).

6 $H\beta_{BC}$ PROFILE SHAPE

6.1 The influence of M and L/M

We generated median $H\beta_{BC}$ profiles in bins covering narrow ranges of derived M and L/M. The adopted binning is shown in Fig. 7. The median spectra (normalized to the local continuum) are plotted in Fig. 8. Table 2 provides, for every bin, average measures of the $H\beta_{BC}$ profile centroid at a quarter and half peak intensity, the best fit to the profile shape, and the intensity ratio (C2/C1) in the case when two components have been used.

The median $H\beta_{BC}$ profile computed for each bin (see Figs 9 and 10) suggests the following:

(i) A Lorentz function provides good fits to median profiles in bins for which $3.9 < \log L/M < 4.4$, and for $3.4 < \log L/M < 3.9$ and $7.5 < \log M < 8.5$. Profile models employing Gaussian functions yield poorer fits with significantly larger χ^2. The slight redward asymmetry in the bin $3.9 < \log L/M < 4.4$ and $8.5 < \log L/M < 9.5$ can be modelled by adding a weak, redshifted Gaussian

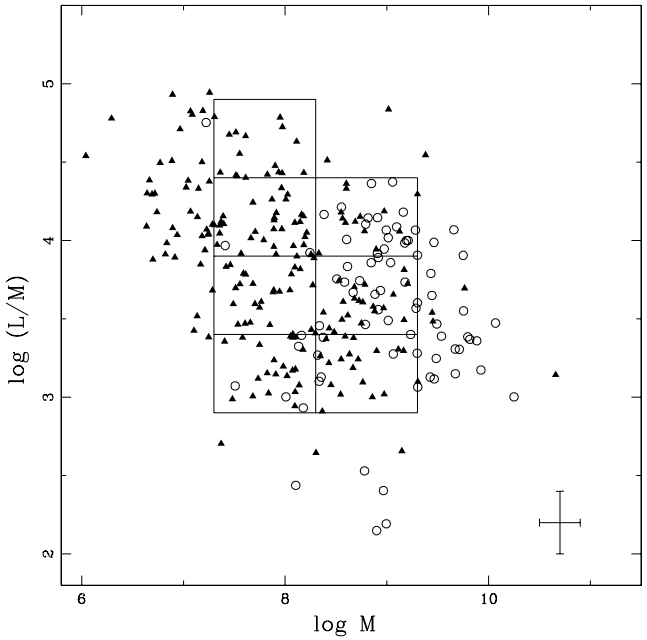

Figure 7. Binning of our sample in the L/M versus M parameter space for the median spectra computations. Symbols are as in Fig. 1.

component C2 with C2/C1 $\approx$ 0.1. Similar considerations apply to the bin $4.4 < \log L/M < 4.9$ and $7.5 < \log M < 8.5$ (i.e. largest L/M, possibly super-Eddington, and lowest M) profile: a slight blueward asymmetry visible in the median profile can be modelled as an additional, blueshifted component contributing $\sim$0.1 of the total line emission.

(ii) If $\log L/M < 3.4$, profiles are better fitted with double Gaussian models than using a Lorentz core plus broader Gaussian component. The latter model is favoured if the narrow component of Hβ is *not* subtracted (e.g. Oshlack et al. 2002), but lack of narrow component subtraction will also lead to an underestimate of M.

(iii) The 'red shelf' or redshifted Gaussian component – we refer to it as a very broad line region (VBLR) component – appears to be strongly influenced by M, i.e. larger M sources show a more prominent VBLR component, as well as by L/M (this is especially evident from the values for $8.5 < \log M \leqslant 9.5$ reported in Table 2). The M dependence is easily seen by comparing the solid (lower mass) and overlaid dashed (higher mass) profiles in each frame of Fig. 8. Table 2 shows that $c(1/4)$ measures are significantly redshifted for the bins corresponding to larger M.

Best fits to H$\beta_{\rm BC}$ and individual line components are shown in Fig. 9. Fig. 10 illustrates a case in which the exchange from a Lorentzian to a Gaussian significantly worsen residuals. The case shown is the one where fits provide more similar results. In general, exchanging functional forms from the best-fitting ones implies larger differences and a χ^2 worsening by a factor of $\approx$2.

6.2 Influence of radio loudness on H$\beta_{\rm BC}$

Is the H$\beta_{\rm BC}$ profile shape influenced by radio loudness? To answer this question, we generated the H$\beta_{\rm BC}$ profile (see Fig. 11) for the interval $8.5 < \log M < 9.5$ and *any* L/M for RQ and RL separately ($N_{\rm RQ} = 56$, $N_{\rm RL} = 36$). Fig. 11 shows that the composite spectra of RL and RQ objects are different: the narrow lines ([O III] $\lambda\lambda$4959,5007 and H$\beta_{\rm NC}$) are stronger and W(H$\beta_{\rm BC}$) is lower in RL objects. At the same time, the H$\beta_{\rm BC}$ profiles remain indistinguishable within our S/N limits (see Fig. 11). To check this result further, we additionally generated the composite spectra separating RL and RQ objects in three other M and L/M ranges: (a) $8.5 < \log M < 9.5$ and $3.9 < \log L/M < 4.4$($N_{\rm RQ} = 14$, $N_{\rm RL} = 19$); (b) $8.5 < \log M < 9.5$ and $3.4 < \log L/M < 3.9$ ($N_{\rm RQ} = 26$, $N_{\rm RL} = 13$); and (c) $8.0 < \log M < 9.0$ and $3.9 < \log L/M < 4.4$ ($N_{\rm RQ} = 14$, $N_{\rm RL} = 19$). Although the S/N ratio of the composites was lower since fewer objects were used, results were similar: indistinguishable H$\beta_{\rm BC}$ profiles and centroids, with higher W([O III] $\lambda\lambda$4959,5007) and lower W(H$\beta_{\rm BC}$) for RL objects. We conclude that the H$\beta_{\rm BC}$ line profile shape does not depend strongly on radio loudness.

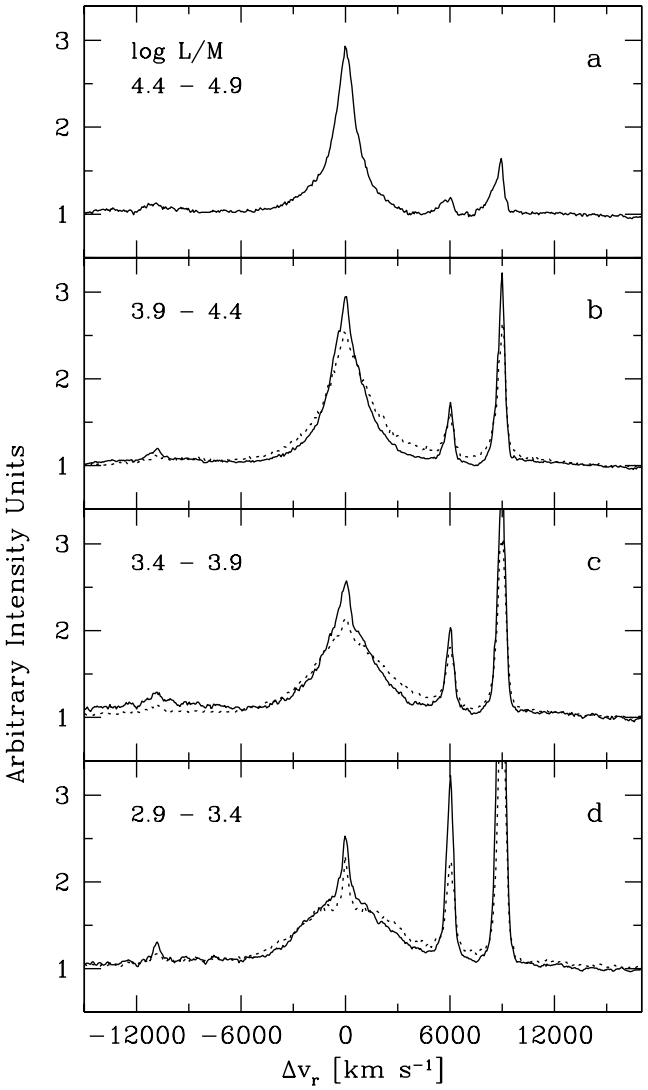

Figure 8. Hβ line profiles after Fe II$_{\rm opt}$ subtraction. From top to bottom the plots correspond to: (a) $\log L/M = 4.4$–4.9; (b) $\log L/M = 3.9$–4.4; (c) $\log L/M = 3.4$–3.9; (d) $\log L/M = 2.9$–3.4. Note that $\log L/M \approx 4.53$ corresponds to $L/L_{\rm Edd} \approx 1$. Solid lines correspond to $7.3 \leqslant \log M \leqslant 8.3$, and dashed lines to $8.3 < \log M \leqslant 9.3$.

7 THE 'BLUE OUTLIERS'

7.1 Spectral properties of [O III] $\lambda\lambda$4959,5007 'blue outliers'

In a previous investigation (Zamanov et al. 2002), we identified seven objects from the M03 sample that showed an [O III]

Table 2. Hβ_{BC} line centroids at a quarter and a half fractional intensity as a function of $\log L/M$. For each interval of $\log L/M$ the table reports the Hβ_{BC} best-fitting function (FF), either Lorentzian (L) or Gaussian (G), and their peak position and FWHM. In case two components are needed for the best fit, their intensity ratio (C2/C1) is reported in the last column.

$\log L/M$	$c(1/4)$	$c(1/2)$	FWHM	Best fit						C2/C1
				1st component			2nd component			
				FF	Peak	FWHM	FF	Peak	FWHM	
	(km s^{-1})	(km s^{-1})	(km s^{-1})		(km s^{-1})	(km s^{-1})		(km s^{-1})	(km s^{-1})	
$7.5 \leqslant \log M \leqslant 8.5$										
4.4–4.9	-170^{+290}_{-390}	-55^{+120}_{-110}	1410 ± 110	L	50	1400	G	−1850	2100	0.09
3.9–4.4	$+140^{+400}_{-390}$	$+80^{+160}_{-160}$	2310 ± 160	L	−5	2350	...	...	...	...
3.5–3.9	$+140^{+500}_{-540}$	$+200^{+240}_{-240}$	3200 ± 240	L	50	3500	...	...	...	...
2.9–3.4	$+400^{+780}_{-600}$	-85^{+310}_{-310}	5490 ± 310	G	−320	4000	G	+1400	10000	0.73
$8.5 < \log M \leqslant 9.5$										
3.9–4.4	$+330^{+620}_{-560}$	$+250^{+250}_{-240}$	3100 ± 250	L	+1	3000	G	+4000	7600	0.12
3.5–3.9	$+915^{+1100}_{-790}$	$+440^{+320}_{-320}$	4900 ± 320	G	−20	2900	G	+1050	8700	1.7
2.9–3.4	$+2320^{+1060}_{-1090}$	$+314^{+400}_{-380}$	7000 ± 400	G	−70	4900	G	+2100	12600	1.09

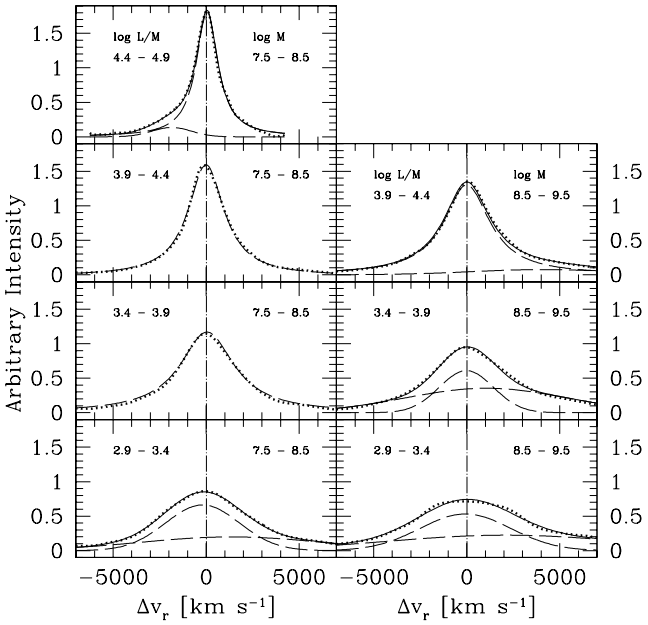

Figure 9. Hβ_{BC} line profile fitting after continuum, Fe II$_{opt}$ and Hβ_{NC} subtraction for the intervals in $\log L/M$ and M defined in Table 2. The 'cleaned' Hβ_{BC} (dotted line) is shown along with single fitting components (dashed lines) and with the resulting best fit (thin solid line).

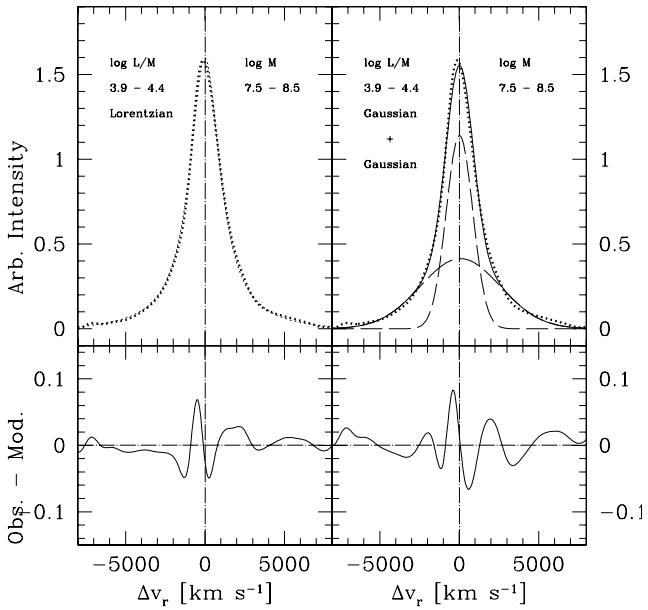

Figure 10. Example of Hβ_{BC} line profile fitting with different functional forms. The upper panels show the Hβ_{BC} (dotted lines) fit by a Lorentzian (left, best fit identical to Fig. 9) and to a double Gaussian. The lower panels show residuals for both cases. The Lorentzian fit is significantly better, yielding a decrease in χ^2 by a factor of ≈1.5. This is the most doubtful case among the ones considered in this study; in all other cases a Lorentzian/Gaussian exchange from best fits yields a χ^2 worsening by a factor of ≈2.

λλ4959,5007 blueshift relative to the peak of Hβ. The shift amplitudes were $\geqslant$250 km s^{-1}, leaving little doubt that we are observing a significant velocity displacement. We have identified five additional AGN that show large-amplitude blueshifts among the objects of G99. Some properties of all of these sources are given in Table 3. All of the sources show strong Fe II$_{opt}$ emission. In the E1 context they show: (1) $R_{Fe\,II} \gtrsim 0.5$; (2) FWHM(Hβ) < 4000 km s^{-1} (i.e. they are located in spectral bins A2 and A3 of Sulentic et al. 2002); and (3) a large C IV λ1549 broad component blueshift (Zamanov et al. 2002). Blue outliers also show weak [O III] λλ4959,5007 emission with W([O III] λ5007) $\lesssim$ 20 Å, and a median value of ≈6 Å.

Nine out of our 12 outliers are formally NLSy1s. In general, the [O III] λλ4959,5007 lines of NLSy1s have a relatively narrow profile with often, in addition, a second broader, blueshifted component (Véron-Cetty, Véron & Gonçalves 2001). The blueshift is 400–1100 km s^{-1} when the two components can be deblended (Zheng et al. 2002). These values correspond to the blue outliers range, suggesting that the latter are an extreme subset with low W([O III] λ5007) when only the shifted component is visible.

7.2 FWHM of Fe II$_{opt}$ and [O III] λλ4959,5007 lines

Computation of M requires that Hβ_{BC} be separated from any narrow component so that FWHM(Hβ_{BC}) can be properly measured. The problem is that extreme sources like the blue outliers show no profile inflection (reflected in the fact that they are well fitted by a Lorentzian function). The rationale for our methodology has been

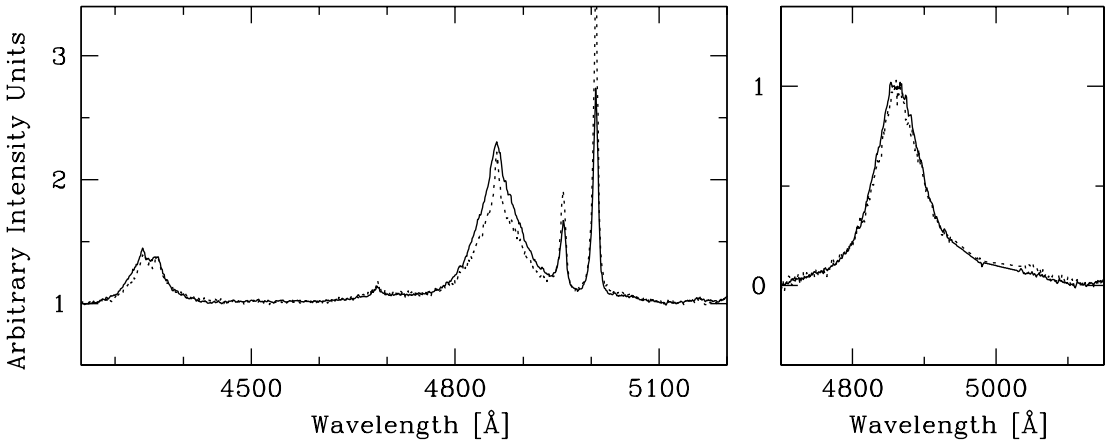

Figure 11. Comparison of the RQ and RL objects in the mass interval $8.5 < \log M < 9.5$ and any L/M ratio ($N_{\rm RQ} = 56$, $N_{\rm RL} = 36$). (left) Comparison of the composite spectra of RQ and RL (after subtraction of the Fe II$_{\rm opt}$ template). W(H$\beta_{\rm BC}$) is 20 per cent higher in RQ, W([O III] λ5007) is 35 per cent higher in RL. (right) Cleaned and scaled H$\beta_{\rm BC}$ profile. The H$\beta_{\rm BC}$ profiles of RQ and RL are almost identical.

Table 3. The spectral properties of the 'blue outliers': radial velocity difference between the top of Hβ and [O III] λ5007, the equivalent width and FWHM of [O III] λ5007, the FWHM of H$\beta_{\rm BC}$ and Fe II λ4570, and the equivalent width ratio of Fe II λ4570 and H$\beta_{\rm BC}$($R_{\rm Fe\,II}$).

Name	Δv (km s^{-1})	W([O III] λ5007) (Å)	FWHM([O III]) (km s^{-1})	FWHM(Hβ) (km s^{-1})	FWHM(Fe II) (km s^{-1})	$R_{\rm Fe\,II}$
I Zw 1	−640	15.3	1440 ± 120	1090	1100	1.30±0.1
PKS 0736+01*	−430	2.6	720 ± 60	3260	3560	0.70±0.1
PG 0804+761	−305	10.1	780 ± 60	3300	3100	0.42±0.1
PG 1001+291	−680	3.4	960 ± 60	1760	1600	0.71±0.1
PG 1402+261	−300	2.6	900 ± 180	1940	2000	0.73±0.1
PG 1415+451	−600	2.9	660 ± 60	2560	2870	0.66±0.1
PG 1543+489	−950	6.5	–	1560	1600	0.64±0.1
RX J0136.9−3510	−380	6.0	900 ± 60	1050	1100	1.0±0.1
RX J0439.7−4540	−580	5.0	1020 ± 120	1020	1100	0.9±0.1
RX J2217.9−5941	−330	8.1	1140 ± 120	1370	1600	2.0±0.2
RX J2340.6−5329	−490	21.8	780 ± 60	1230	1600	1.3±0.1
MS 2340.9−1511	−420	5.8	780 ± 60	970	1200	1.1±0.1

*RL CD source.

detailed in M03, and will not be discussed again here. We just recall that we normally assume (and find) that the narrow component of Hβ shows almost the same shift and width properties as the [O III] $\lambda\lambda$4959,5007 lines. However, in blue outliers W([O III] λ5007) is smaller than in any broad emission-line AGN class and is also blueshifted relative to the peak of Hβ. We conclude that we are not measuring a narrow-line component at the Lorentzian tip of the Hβ profile. Any narrow component of Hβ is assumed to be blueshifted and lost in the blue wing of the broad line – even assuming it has the same strength as [O III] λ5007 in blue outliers, it would represent less than 10 per cent of the total line flux. Subtraction of a narrow Hβ component would have a non-negligible effect on the FWHM(H$\beta_{\rm BC}$) measurement which is needed for the M estimation.

The Fe II λ4570 feature is a complex of lines thought to have FWHM similar to H$\beta_{\rm BC}$. We estimated FWHM(Fe II λ4570) *independently* from FWHM(H$\beta_{\rm BC}$) by Fe II$_{\rm opt}$ template fitting using the I Zw 1 spectrum (of course, only for highest S/N spectra; see M03 for details). In our sample FWHM(Fe II λ4570) is similar to FWHM(H$\beta_{\rm BC}$) with few exceptions only (see Bongardo et al. 2002). Estimated FWHM(Fe II λ4570) values are given in Table 3. No narrow Fe II λ4570 component has been detected and nor is one expected given the low inferred density for the narrow-line region. In principle, we can use FWHM(Fe II λ4570) instead of FWHM(H$\beta_{\rm BC}$) in the mass derivations in order to avoid any error associated with a narrow-line component. Use of FWHM(Fe II λ4570) instead of FWHM(H$\beta_{\rm BC}$) will yield M values within ∼10 per cent of ones derived from FWHM(H$\beta_{\rm BC}$).

The correlation of nuclear black hole (BH) mass with stellar bulge velocity dispersion σ_* is now well established in nearby galaxies. Recent results (Nelson 2000; Boroson 2002) show that a BH mass–FWHM([O III] λ5007) correlation is also present but with larger scatter. The FWHM([O III] λ5007) measures given in Table 3 provide another way to estimate BH masses. The derived values are, however, considerably higher than values calculated using FWHM(H$\beta_{\rm BC}$) and source luminosity. This is not surprising because NLSy1-type AGN apparently do not follow Nelson's relation (Mathur, Kuraszkiewicz & Czerny 2001). If NLSy1s do not follow the relation, then blue outliers will almost certainly show the same lack of agreement. This does not contradict our assumption that blueshifted [O III] $\lambda\lambda$4959,5007 arise in outflowing gas (Zamanov et al. 2002), possibly associated with a disc wind. The [O III] $\lambda\lambda$4959,5007 region in blue outliers may be very compact and its velocity field is not likely to be dynamically related to the host-galaxy stellar bulge. This points to a limiting W([O III] λ5007)

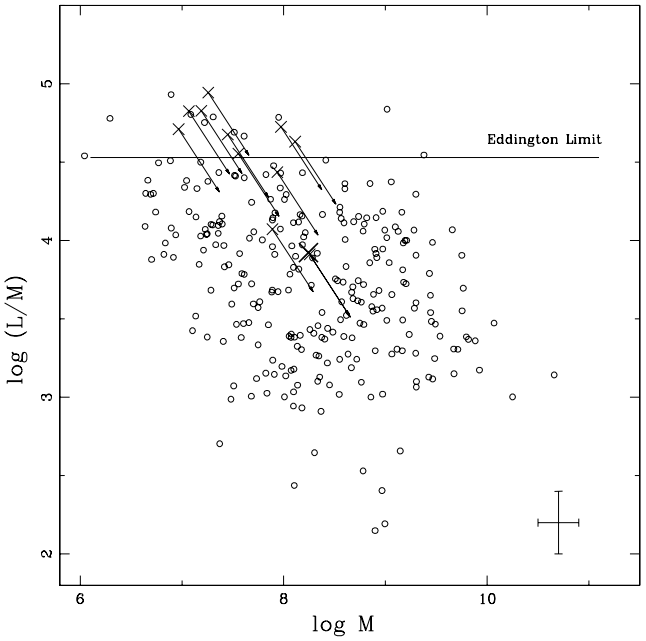

Figure 12. Position of blue outliers (small crosses) relative to other sources in our sample (open circles). The larger cross indicates the position of PKS 0736+01 – the only known RL 'blue outlier'. The dashed line indicates the Eddington limit. Arrows indicate displacements of blue outliers if we apply an orientation correction ∼0.4 to the derived masses. Blue outliers are among the highest L/M sources and remain in the upper part of the diagram even after an orientation correction. One should consider that many other sources would move in the same direction of the blue outliers if a proper orientation were applied to all sources.

(≈20 Å), below which FWHM([O III] λλ4959,5007) emission ceases to be a useful mass estimator.

7.3 M_B and L/M ratio of [O III] outliers

All blue outliers lie in the region of E1 thought to be populated by highly accreting (high L/M) sources (Marziani et al. 2001). Most of them are located close to the Eddington limit ($\log L/M \approx 4.53$, see Fig. 12). This is also true if: (1) FWHM(Fe II λ4570) is used instead of FWHM($H\beta_{BC}$) to derive M, and (2) an orientation correction is applied. The blue outliers may be oriented close to pole-on. Since $M \propto \mathrm{FWHM}^2$, an inclination correction will move the 'blue outliers' towards higher mass and lower L/M (see the arrows on Fig. 12). Even with an inclination correction by a factor ≈4, the L/M values for blue outliers remain among the highest observed. We note that: (1) other sources should also be corrected for orientation, especially if low ionization lines are emitted in a flattened configuration in all Population A sources, as suggested by (Marziani et al. 1996); and (2) some care is needed, since we neglected a photometric correction that is basically unknown. We do not know whether any sort of continuum beaming operates for RQ AGN as $i \rightarrow 0^\circ$ [very similar $W(H\beta_{BC})$ for CD and LD RL sources suggests no strong effect (Sulentic et al. 2003)]. Observational errors and uncertainty in the orientation correction do not allow us to determine whether some blue outliers are really super-Eddington sources as they appear in Fig. 12.

All blue outliers show estimated masses less than $10^{8.5}$ $M_\odot$. We tried to determine if the large L/M of blue outliers was a consequence of a low-mass bias by calculating the M_B difference between blue outliers and other sources in two mass ranges: (1) $7.15 \leqslant \log M \leqslant 8.45$ (where the 'blue outliers' are before the orientation correction) and (2) $7.55 \leqslant \log M \leqslant 8.85$ (where they move after the orientation correction). Table 4 shows that the blue outliers are almost certainly ∼1 mag brighter than other sources with similar mass, implying 2–3 times higher L/M ratios.

Table 4. M_B of the 'blue outliers' (as they are given in the Véron-Cetty & Véron (2001) catalogue without correction for the cosmology), compared with other objects in the sample with similar mass. P_{KS} is the probability that the 'blue outliers' and the other objects in the indicated mass ranges are randomly drawn from the same parent population according to Kolmogorov–Smirnov test.

	Ave. $\pm\sigma$	Med. $^{75\mathrm{percent}}_{25\mathrm{percent}}$	P_{KS}
Blue outliers	-23.9 ± 0.8	$-23.85^{-23.45}_{-24.30}$	
$7.0 \leqslant \log M \leqslant 8.2$	-22.4 ± 0.8	$-22.20^{-21.50}_{-23.40}$	0.00035
$7.6 \leqslant \log M \leqslant 8.8$	-22.8 ± 0.8	$-22.90^{-21.80}_{-23.90}$	0.00600

8 DISCUSSION

8.1 Mass–luminosity diagram

The ranges of M and L/M considered in this study are similar to those in other recent work (Woo & Urry 2002a; Collin et al. 2002). We find that the Eddington limit defines an approximate upper boundary to the luminosity distribution (as in Woo & Urry 2002a), indicating that there are no known low-z AGN accreting significantly above the Eddington limit (this depends on the adopted H_0 value). Fig. 1 also suggests that there may be fewer high- (than low-) mass sources with L/M close to the Eddington limit. This might be a selection effect or an indication that galaxies with a high-mass BH may be unable to supply fuel at high L/M. In other words, the upper envelope in Fig. 1 might be due to the Eddington limit as well as the ability of the surrounding matter to feed the accretion flow (see e.g. Nicastro, Martocchia & Matt 2003). The lower envelope of the luminosity distribution may be due to a selection effect (e.g. Woo & Urry 2002a), or it may indicate that only sources radiating at 0.01 $(L/L_{Edd}) \lesssim 1.00$ exhibit a stable broad-line region. The latter possibility might be connected with the presence/absence of an accretion disc wind (see also Kollatschny & Bischoff 2002).

8.2 On the difference between radio-loud and radio-quiet AGN

Somewhat confusing claims have recently been made on the difference between RL and RQ sources in terms of M and L/M. Laor (2000) found that the radio loudness is strongly related to M. Woo & Urry (2002b) concluded that radio loudness does not depend strongly on M. Lacy et al. (2001) found no evidence for critical M or L/M ratio that turns on powerful radio jets. Ho (2002) showed that the dependence of radio loudness on M disappears altogether when one considers AGN with a broad range of intrinsic luminosity. At the same time he found that radio loudness seems to be related to the mass accretion rate. RL and RQ sources are well separated *in terms of M* by the new eigenvector analysis of Boroson (2002).

The difference between RQ and RL on eigenvectors diagram (Boroson 2002) is probably connected with the inclusion of [O III] λ5007 line parameters. In RL quasars, part of the [O III] λλ4959,5007 comes from extended regions connected with the radio jet (Wilman,

Johnstone & Crawford 2000). Previous work has shown that RL activity in low-M sources may be physically possible. Our sample contains a RL NLSy1 that is one of the highest L/M sources, and other sources that radiate at $\log L/M \approx 4.5$. Our analysis stressed that there are no appreciable effects (within the limits set by our S/N) on the H$\beta_{\rm BC}$ profile attributable to radio loudness, and that Population B RL and RQ sources can have the same M and L/M values. Therefore, it is not unreasonable to conclude that *a similar range of M and L/M is physically possible for both RQ and RL sources*. However, this does not mean that the mass functions for RL and RQ sources are necessarily the same. A robust inference from the bootstrap analysis reported in Section 5.1 is that the mass function and the conditional probability of having certain L/M values at fixed M are likely to be different for the two AGN classes. A correct estimation of the mass function and of the L/M probability distribution demands a more thorough analysis that includes selection biases. In addition, the RL/RQ dichotomy is probably related to parameters other than M and L/M, such as BH spin and morphological segregation. We suggest that the intrinsic mass function and L/M distribution differences as well as jet-related effects like [O III] $\lambda\lambda$4959,5007 enhancement in RL sources and sample selection criteria may drive the RQ/RL separation shown by Laor (2000) and Boroson (2002).

8.3 Transition in H$\beta_{\rm BC}$ line profile shape

Connecting empirical and physical parameters, we find that median profiles for H$\beta_{\rm BC}$ in Population A sources ($\log L/M > 3.9$ and for $3.5 < \log L/M < 3.9$ and $7.5 < \log L/M < 8.5$) show a Lorentzian shape. In other words, if $\log L/M \gtrsim 3.9$, the shape is Lorentzian for all values of M. Similarly, if $\log L/M \lesssim 3.4$ (bins dominated by Population B sources), the profile is redward asymmetric and can be decomposed into two Gaussian components (one redshifted and the other not). This suggests that the transition from Lorentzian to double Gaussian profiles is governed by a critical L/M value (it is interesting to note that the H$\beta_{\rm BC}$ asymmetry is also one of the major correlates of the original E1 of Boroson & Green 1992). Unfortunately, the division of the bins in the L/M strip $3.4 < \log L/M < 3.9$ did not make the situation clearer. We conclude that the Lorentzian–double Gaussian profile transition occurs between $3.4 \lesssim \log L/M \lesssim 3.9$ ($0.08 \lesssim L/L_{\rm Edd} \lesssim 0.25$). A more precise value would require knowledge of source orientation effects and a better-constrained α value. This provides a physical basis for the phenomenological finding about profile change at FHWM(H$\beta_{\rm BC}$) ≈ 4000 km s^{-1} and the resulting Population A–B hypothesis (Sulentic et al. 2002).

8.3.1 c(1/4) Hβ$_{\rm BC}$ dependence on mass: not only gravitational redshift

We remark that a double Gaussian fit to H$\beta_{\rm BC}$ in Population B sources is a formal result: two components are required to account for the redward asymmetry. The two components have a physical justification if, for example, the broader (VBLR) one can be ascribed to gas that lies closest to the continuum source in an optically thin (to the H I ionizing continuum) region with large covering factor $f_{\rm c} \approx 1$ (as defined in Marziani & Sulentic 1993; Brotherton 1996). A new result from this investigation is that the amplitude of the redward asymmetry is mass-dependent.

The $c(1/4)$ dependence on M [for $\Delta\log M \approx 1$ we obtain a factor $\approx$6 increase in the $c(1/4)$ redward displacement] means that we can try to ascribe the presence of the 'red shelf'/VBLR component and the redward asymmetry to gravitational and transverse redshift (e.g. Corbin 1997). If the VBLR redshift is gravitational and transverse, taking the $c(1/4)$ value as a conservative estimate, we obtain the following distances from the central continuum source for the line-emitting gas: if $3.5 \lesssim \log L/M \lesssim 3.9$, then $r \approx 0.005$ pc and 0.01 pc for $\log M = 8$ and $\log M = 9$ respectively. In the case of the largest VBLR redshifts, the shift in radial velocity is $\Delta v_{\rm r} \approx 2300$ km s^{-1} and we find $r \approx 0.015$ pc ≈ 170 gravitational radii for $\log M = 9$. If we model the VBLR gas as a shell ($f_{\rm c} \approx 1$) with optical depth to the Lyman continuum $\tau \lesssim 1$, a CLOUDY (Ferland 2000) simulation shows luminosity of Hβ, $\log L({\rm H}\beta)_{\rm VBC} \approx 41.7$, where the line luminosity is in erg s^{-1}. This falls far short in explaining the VBLR luminosity for sources in bin $3.5 < \log L/M < 3.9$, $8.5 < \log M < 9.5$. The average $\overline{\log L}({\rm H}\beta_{\rm BC})$ is 43.08. The VBLR contributes two-thirds of the total, so the VBLR average luminosity is $\overline{\log L}({\rm H}\beta)_{\rm VBC} \approx 42.9$. The difference between the expected and observed VBLR luminosity is largely a consequence of the small shell radius required to explain the large $\Delta v_{\rm r}$ in the $c(1/4)$. In addition, the assumption of $c(1/4)$ being dominated by gravitational plus transverse redshift implies that $z_{\rm grav} \approx (3/2)({\rm FWHM}/c)^2$, which is not observed. We conclude that, even if $c(1/4)$ is mass-dependent, the $c(1/4)$ shift amplitude cannot be explained by gravitational plus transverse redshift *alone*. Once the stringent (and perhaps unphysical) distances from the central continuum sources set by gravitational redshift are relaxed, we note that our VBLR model can explain Hβ VBLR luminosity with reasonable shell radii. While this issue requires further investigation, it is tempting to suggest that we may be observing the long-sought infall, and that we are observing it easily because of the low optical depth expected also along the line of sight to Hβ. This would straightforwardly explain the ubiquitous presence of strong H$\beta_{\rm BC}$ redward asymmetries at low L/M.

8.4 On the nature of the blue outliers

We observe 'blue outliers' (following the simple wind model of Zamanov et al. 2002) when the [O III] $\lambda\lambda$4959,5007 lines and the peak of Hβ arise in different regions – Hβ from a near face-on accretion disc and [O III] from a wind with velocity of about 1000 km s^{-1}. In terms of orientation these RQ sources would be analogous to some CD RL quasars or even to BL Lacs (blazars). Other nearly as large L/M oriented sources can/must exist in our sample but they are not 'blue outliers' for at least two reasons: (i) they possess a well-developed narrow-line region (NLR), which is unlikely to show a significant blue-shifted component; and (ii) they are not oriented face-on. There are probably also lower L/M sources oriented face-on; however, their L/M ratio may not be sufficient to power a wind or the wind outflow velocity may be low (roughly <300 km s^{-1}). This could explain why the blue outliers are exclusively sources with very high L/M. It is worth noting that the only RL blue outlier, PKS 0736+01, is a flat-spectrum radio source, and one of the brightest high polarization, optically violently variable sources. Its optical continuum is dominated by a 'blazar' component as in BL Lacs (Malkan & Moore 1986). Continuum properties suggest relativistic beaming, making this a true pole-on RL source consistent with the interpretation of the 'blue outliers' proposed by Zamanov et al. (2002).

In the most recent scenarios for joint AGN and galaxy evolution (e.g. Granato et al. 2001), the active nucleus and the galaxy evolve together, with BH accreting matter and the galaxy making stars and supplying fuel for the quasar. At some point, the wind from the accreting BH blows away the matter surrounding it and a quasar emerges. The central accretion source then appears as an unobscured

quasar, which lasts as long as there is fuel in the accretion disc (Fabian 1999). In this scenario our 'blue outliers' could represent the stage when the quasar has just emerged [cf. Krongold, Dultzin-Hacyan & Marziani (2001) for a similar interpretation stemming from the analysis of NLSy1 host galaxies and environment]. They could be in the process of building of their NLR.

9 CONCLUSIONS

In this paper we computed virial masses and Eddington ratios for a sample of ∼300 AGN. We have shown that L/M seems to govern the overall shape of the H$\beta_{\rm BC}$, and we found an interesting dependence on M of the H$\beta_{\rm BC}$ asymmetry. The transition between sources showing Lorentzian and double Gaussian H$\beta_{\rm BC}$ profiles is probably associated with a critical L/M value, as suggested by Sulentic et al. (2002). L/M and M values in the range $8 \lesssim M \lesssim 9.5$ and $3 \lesssim \log L/M \lesssim 4.2$ are found likely for both RL and RQ AGN, while others ($\log L/M \gtrsim 4.2$) may be very unlikely for RL sources. However, it is important to stress the existence of a radio-loud blue outlier radiating at very high L/M ($\log L/M \approx 4.8$; other RL sources radiate at $\log L/M \approx 4.4$). This shows that there is no physical impossibility for RL sources to be of large L/M and small M; they may simply be less likely to be that way.

We confirm that the 'blue outliers' are mainly NLSy1 sources (Zamanov et al. 2002; see also Sulentic et al. 2000a). We increase the number of known 'blue outliers' to 12. We show that all blue outliers are accreting at two times higher Eddington ratio than other sources with similar mass. The compactness of their NLR points towards very young ages (Zamanov et al. 2002), suggesting that they may be 'fledgling' AGN as discussed for NLSy1s by Sulentic et al. (2000a) and Mathur (2000). An interesting issue is then whether different M and L/M distributions may point towards evolutionary effects, i.e. whether some RQ sources may be the parent population for all quasars (for example, NLSy1s, 'extreme Population A' sources, may evolve into Population B RQ or even RL depending on accretion of angular momentum and/or host galaxy type/evolution).

In the future we will need an orientation indicator for each individual AGN. This is very important for a correct evaluation of M. The C IV λ1549 line profile shows promise as an orientation indicator, at least for Population A sources (Richards et al. 2002). It may also provide us with important clues about aspects of broad-line region structure and its dependence on L/M, and ultimately, with a 3D observational space to map uniquely into a 3D 'physical' parameter space defined by M, L/M and orientation.

ACKNOWLEDGMENTS

The authors acknowledge support from the Italian Ministry of University and Scientific and Technological Research (MURST) through grant Cofin 00-02-004. We also wish to thank Giovanna Stirpe for fruitful discussions and a careful reading of the manuscript. This research has made use of the NASA/IPAC Extragalactic Database (NED), which is operated by the Jet Propulsion Laboratory, California Institute of Technology, under contract with the National Aeronautics and Space Administration.

REFERENCES

Bongardo C., Zamanov R., Marziani P., Calvani M., Sulentic J. W., 2002, in Cagnoni I., ed, AGN5: Inflows, Outflows and Reprocessing Around Black Holes, 15 (www.unico.it/ilaria/AGN5/proceedings.html)
Boroson T., 2002, ApJ, 565, 78
Boroson T. A., Green R. F., 1992, ApJS, 80, 109
Boroson T. A., Persson S. E., Oke J. B., 1985, ApJ, 293, 120
Brotherton M. S., 1996, ApJS, 102, 1
Collin S., Boisson C., Mouchet M., Dumont A.-M., Coupé S., Porquet D., Rokaki E., 2002, A&A, 388, 771
Corbin M. R., 1997, ApJ, 485, 517
Dultzin-Hacyan D., Marziani P., Sulentic J. W., 2000, Rev. Mex. Astron. Astrofis. Conf. Ser., 9, 308
Efron B., Tibshirani R. J., 1993, An Introduction to the Bootstrap (Monographs on Statistics and Applied Probability, Vol. 57). Chapman & Hall, New York
Elvis M. et al., 1994, ApJS, 95, 1
Fabian A. C., 1999, MNRAS, 308, L39
Ferland G. J., 2000, Rev. Mex. Astron. Astrofis. Conf. Ser., 9, 153
Gaskell C. M., Brandt W. N., Dietrich M., Dultzin-Hacyan D., Eracleous M., 1999, ASP Conf. Ser. Vol. 175, Structure and Kinematics of Quasar Broad Line Regions. Astron. Soc. Pac., San Francisco
Granato G. L., Silva L., Monaco P., Panuzzo P., Salucci P., De Zotti G., Danese L., 2001, MNRAS, 324, 757
Grupe D., Beuermann K., Mannheim K., Thomas H.-C., 1999, A&A, 350, 805 (G99)
Ho L. C., 2002, ApJ, 564, 120
Jarvis M. J., McLure R. J., 2002, MNRAS, 336, 38
Kaspi S., Smith P. S., Netzer H., Maoz D., Jannuzi B. T., Giveon U., 2000, ApJ, 533, 631
Kollatschny W., Bischoff K., 2002, A&A, 386, 19
Krongold Y., Dultzin-Hacyan D., Marziani P., 2001, AJ, 121, 702
Lacy M., Laurent-Muehleisen S. A., Ridgway S. E., Becker R. H., White R. L., 2001, ApJ, 551, L17
La Franca F., Gregorini L., Cristiani S., de Ruiter H., Owen F., 1994, AJ, 108, 1548
Laor A., 2000, ApJ, 543, L111
McLure R. J., Kukula M. J., Dunlop J. S., Baum S. A., O'Dea C. P., Hughes D. H., 1999, MNRAS, 308, 377
Malkan M. A., Moore R. L., 1986, ApJ, 300, 216
Marziani P., Sulentic J. W., 1993, ApJ, 409, 612
Marziani P., Sulentic J. W., Dultzin-Hacyan D., Calvani M., Moles M., 1996, ApJS, 104, 37
Marziani P., Sulentic J. W., Zwitter T., Dultzin-Hacyan D., Calvani M., 2001, ApJ, 558, 553
Marziani P., Zamanov R., Sulentic J. W., Calvani M., Dultzin-Hacyan D., 2003a, Mem. Soc. Astron. Ital., 74, 492
Marziani P., Sulentic J. W., Zamanov R., Calvani M., Dultzin-Hacyan D., Bachev R., Zwitter T., 2003b, ApJS, in press (M03)
Mathur S., 2000, New Astron. Rev., 44, 469
Mathur S., Kuraszkiewicz J., Czerny B., 2001, New Astron., 6, 321
Murray N., Chiang J., Grossman S. A., Voit G. M., 1995, ApJ, 451, 498
Nagao T., Taniguchi Y., Murayama T., 2000, AJ, 119, 260
Nelson C. H., 2000, ApJ, 544, L91
Nicastro F., 2000, ApJ, 530, L65
Nicastro F., Martocchia A., Matt G., 2003, ApJ, 589, L13
Oshlack A. Y. K. N., Webster R. L., Whiting M. T., 2002, ApJ, 576, 81
Richards G. T., Vanden Berk D. E., Reichard T. A., Hall P. B., Schneider D. P., SubbaRao M., Thakar A. R., York D. G., 2002, AJ, 124, 1
Schlegel D. J., Finkbeiner D. P., Davis M., 1998, ApJ, 500, 525
Sulentic J. W., Marziani P., Dultzin-Hacyan D., 2000a, ARA&A, 38, 521
Sulentic J. W., Zwitter T., Marziani P., Dultzin-Hacyan D., 2000b, ApJ, 536, L5
Sulentic J. W., Marziani P., Zamanov R., Bachev R., Calvani M., Dultzin-Hacyan D., 2002, ApJ, 566, L71
Sulentic J. W., Zamfir S., Marziani P., Bachev R., Calvani M., Dultzin-Hacyan D., 2003, ApJ, submitted
Véron-Cetty M.-P., Véron P., 2001, A&A, 374, 92
Véron-Cetty M.-P., Véron P., Gonçalves A. C., 2001, A&A, 372, 730
Vestergaard M., 2002, ApJ, 571, 733
Wandel A., Peterson B. M., Malkan M. A., 1999, ApJ, 526, 579

Williams R. J., Pogge R. W., Mathur S., 2002, AJ, 124, 3042
Wilman R. J., Johnstone R. M., Crawford C. S., 2000, MNRAS, 317, 9
Wilson A. S., Colbert E. J. M., 1995, ApJ, 438, 62
Woo J.-H., Urry C. M., 2002a, ApJ, 579, 530
Woo J.-H., Urry C. M., 2002b, ApJ, 581, L5
Zamanov R., Marziani P., 2002, ApJ, 571, L77
Zamanov R., Marziani P., Sulentic J. W., Calvani M., Dultzin-Hacyan D., Bachev R., 2002, ApJ, 576, 9
Zheng X. Z., Xia X. Y., Mao S., Wu H., Deng Z. G., 2002, AJ, 124, 18
Zhou H., Wang T., Dong X., Zhou Y., Li C., 2003, ApJ, 584, 147

This paper has been typeset from a TEX/LATEX file prepared by the author.